PAPER

Correlation of crystal structure and optical properties of $Ba_{0.97}Nd_{0.0267}Ti_{(1-x)}W_xO_3$ perovskite

Z. Raddaoui,[a] B. Smiri,[b] A. Maaoui,[c] J. Dhahri, [ID] *[a] R. M'ghaieth,[b] N. Abdelmoula[d] and K. Khirouni[e]

The $Ba_{0.97}Nd_{0.0267}Ti_{(1-x)}W_xO_3$ (BNT_x) pervoskite with a single phase tetragonal structure was prepared at 900 °C using the Molten salt method. Raman spectra, Fourier transform infrared spectra (FT-IR), absorption spectra (Vis-NIR) and photoluminescence spectra (PL) in the temperature range from 10–300 K were used to investigate the correlations between the crystal structure and the optical properties of BNT_x ceramics. Raman analyses and FT-IR indicated that the W^{6+} ions are incorporated sufficiently into into the BNT_x lattice. The optical absorption spectra were recorded in the wavelength range of 400–1000 nm. The optical band gap (E_g) and Urbach energy (E_u) values were calculated from the absorption spectra. The emission spectra exhibited three prominent peaks located at 880, 1058 and 1340 nm corresponding to the $^4F_{3/2} \rightarrow {}^4I_{9/2,11/2,13/2}$ transition levels, respectively. They also showed a decrease in the intensity of emission spectra following the addition of W^{6+} ions. This decrease is due to the slight changes in the crystal environment around Nd^{3+} and the non-radiative energy transfer. According to the PL measurements, the study of power-excitation density confirmed that two photons at low energy are required to create the down-conversion (DC) emissions, implying that they may also have important applications as DC materials.

1. Introduction

Due to their potential applications in novel multifunctional devices, luminescent materials based on rare earth doped ferro/piezoelectric ceramics have received considerable interest to replace the traditional phosphors in many industrial and commercial technologies, such as solid state lasers, white light-emitting diodes (WLEDs), biomedical imaging, DNA detection, and photodynamic therapy.[1]

However, trivalent neodymium (Nd^{3+}) has emerged as an important RE ion of functional materials in the field of luminescence.[2] The suitability of the Nd^{3+} ion in emitting strong near infrared (NIR) fluorescence makes it a potential candidate for high-power laser applications.[3] Furthermore, most research studies have concentrated on the Nd^{3+} ions due to their efficient

infrared emissions by the three transitions $^4F_{3/2} \rightarrow {}^4I_{9/2}$, $^4F_{3/2} \rightarrow {}^4I_{11/2}$ and $^4F_{3/2} \rightarrow {}^4I_{13/2}$ with emissions at wavelengths around 946, 1064 and 1350 nm which finds potential applications in the fields of laser and infrared optical communications.[4]

Indeed, many studies have demonstrated an appreciable enhancement of the spectral analysis of Nd^{3+} ions. G. Singh *et al.*[5] reports that the emissions of neodymium in lead lanthanum zirconate titanate ($Pb_{0.91}La_{0.08}(Zr_{0.65}Ti_{0.35})_{0.98}O_3$) have been extensively studied owing to their excellent luminescence properties and proper energy separation towards a potential application in the fields of laser and infrared optical communications.[6] Also, K. Lemanski *et al.*[7] discussed the optical properties of $CaTiO_3$ doped by Nd^{3+} ions and studied the influence of luminescent properties as a function of the annealing temperature and the concentration of neodymium ions. It was also demonstrated that the PL intensity of RE ions doped ferroelectric ceramics (Nd^{3+} doped sodium bismuth titanate ($Na_{0.5}Bi_{0.5}TiO_3$)) can be enhanced the polarization as reported that C. He *et al.*[8] Nevertheless, most of the RE ions doped ferroelectric ceramics exhibit only weak luminescence intensity due to the high phonon energy which could increase the possibility of nonradiative transition. To avoid these problems, the development of new materials with low phonon energy ferroelectrics has attracted considerable attention in the last decade.

Currently, Barium Titanate (BT) is one of the most widely used materials, since a significant breakthrough made by its

[a] Laboratoire de la Matière Condensée et des Nanosciences, Université de Monastir, Faculté des Sciences de Monastir, Avenue de l'environnement, 5019 Monastir, Tunisia. E-mail: j.dhahri3000@gmail.com

[b] Laboratoire de Micro-optoélectroniques et Nanostructures, Université de Monastir, Faculté des Sciences Monastir, Avenue de l'environnement, 5019 Monastir, Tunisia

[c] Laboratoire des Interfaces et des Matériaux Avancés, Université de Monastir, Faculté des Sciences de Monastir, Avenue de l'environnement, 5019 Monastir, Tunisia

[d] Laboratoire des Matériaux Ferroélectriques, LR-Physique-Mathématiques et Applications, Université de Sfax, Faculté des Sciences, Route de Soukra km 3.5 B.P 1171, 3000 Sfax, Tunisia

[e] Laboratoire de Physique des Matériaux et des Nanomatériaux Appliquée à L'environnement, Université de Gabes, Faculté des Sciences de Gabes Cité Erriadh, 6079 Gabes, Tunisia
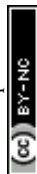
excellent piezoelectric coefficient and a complex photo-luminescent spectrum as reported by Shihua *et al.*[9] This material has a perovskite structure with a direct bandgap (2.8–3.2 eV). It presents many radiative transitions and a visible emission band is found to be sensitive to the particle size whose surface states and crystal lattice defects act as optical absorption centers. Most importantly, BT ceramics have excellent properties including low phonon energy (about 700 cm^{-1}), good insulating property and chemical/physical stability. Therefore, high-efficiency luminescence properties are expected in RE ions doped BT ceramics.

In addition, it had been revealed that the emission intensity of RE ions-doped fluorides and oxides can be modified with the addition of transition metals such as molybdenum (Mo) and tungsten (W).[10,11]

Bokolia *et al.*[12] pointed out that the UC emission intensity of Bi$_4$Ti$_3$O$_{12}$: Er/Yb/W single crystal was significantly enhanced with W doping by a distortion in the crystallographic symmetry. However, few reports on the effects of transition metals on the luminescence properties of RE ions -doped ferroelectric ceramics are found in the literature. Thus, it would be very interesting to investigate the effect of transition metal on the PL emission of RE-ions doped ferroelectric ceramics and their temperature sensing application.

A detailed literature survey shows that not much work has been done on the optical properties and thermo-optical properties in the simultaneous substitution of rare earth Nd^{3+} ion and transition metal W^{6+} in lead-free perovskite. For this reason, we reports on the effect of WO$_3$ on the structural and optical properties of Ba$_{0.97}$Nd$_{0.0267}$TiO$_3$ ceramics.

2. Experimental procedure

2.1. Preparation of Ba$_{0.97}$Nd$_{0.0267}$Ti$_{(1-x)}$W$_x$O$_3$ perovskite samples

The BNT$_x$ ($x = 0.00$ and $x = 0.05$) samples were synthesized *via* a molten salt method using BaCO$_3$, TiO$_2$, WO$_3$ and C$_6$H$_9$NdO$_6$ as precursors, all with a purity better than 99.9%. The precursors were weighed, then, thoroughly mixed in an agate mortar for 2 h. The salt-precursor mixture was placed in an alumina crucible and heated at 800 °C for 24 h. After cooling to room temperature, the mixture was washed with distilled water and filtered to remove the salts. After being dried at 100 °C in air and ground thoroughly, the compounds were pressed into disks (of 8 mm diameter and about 2 mm thickness) and sintered in air at 900 °C for 24 h.

2.2. Characterization of the samples

The Raman spectroscopy was recorded in the frequency range 50–1000 cm^{-1} in a micro-Raman Spectrometer LABRAM HR800. The excitation source was the 633 nm lines of He$^+$ ion laser, working in a back scattering. The spectral resolution of the system was 3 cm^{-1}. The deconvoluted Raman active modes for BaTiO$_3$ and Ba$_{0.97}$Nd$_{0.0267}$Ti$_{(1-x)}$W$_x$O$_3$ ($x = 0.00$ and $x = 0.05$) are determined by fitting using the LabSpec5 software with a combined Lorentzian–Gaussian band shape. Fourier

transform infrared spectra (FT-IR) were recorded in trans-mittance mode at room temperature in the frequency range 450 to 4000 cm^{-1} on PerkinElmer spectrum 100 spectrophotometer using KBr pellet technique. Absorption spectra were recorded *via* a Shimadzu UV-3101PC scanning spectrophotometer. The photoluminescence (PL) measurements were performed in a closed cycle helium cryostat between 10 and 300 K. The 514 nm line of the continuous-wave (cw) Ar$^+$ laser was used as an excitation source. Spectral analysis of the luminescence measurements was carried out using iHR320 monochromator and detected by a Germanium photodetector.

3. Results and discussion

The main panel of Fig. 1 shows the powder X-ray diffraction patterns of Ba$_{0.97}$Nd$_{0.0267}$Ti$_{(1-x)}$W$_x$O$_3$ samples at room temperature. The observed peaks were sharp and with a high intensity, indicating a high crystalline nature. Using Rietveld refinement of the XRD data, we indexed all peaks on the basis of a major tetragonal structure with *P4mm* space group, as well as a BaWO$_4$ secondary phase for $x = 0.05$ sample. Detailed results of the structural parameters deduced from the refinement are summarized in Table 1. As can be seen, a steady variation of the lattice parameters and the volume confirmed the insertion of the doping element (W^{6+} ions) in the titanium site and is explained by the difference of their ionic radius according to Shannon's table.[13]

To get a deep insight into the effect of substitution, Raman spectroscopy is a useful spectroscopic tool for exploring the structure and the presence of functional groups in the host sample. The room temperature depolarized Raman spectra of all Ba$_{0.97}$Nd$_{0.0267}$Ti$_{(1-x)}$W$_x$O$_3$ compositions, are shown in Fig. 2. One can state that Raman spectra of W^{6+}-doped
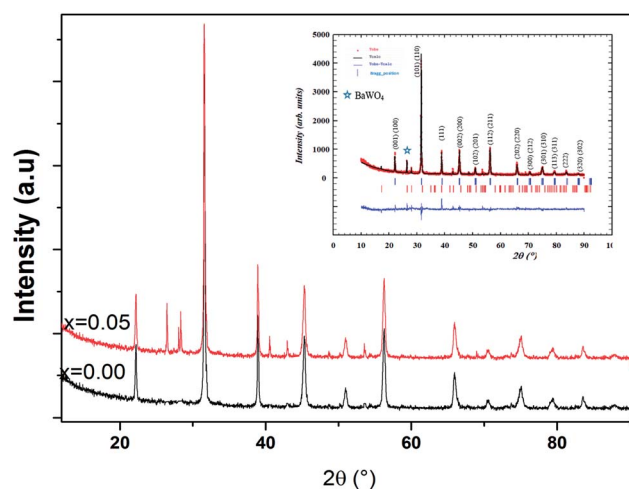

Fig. 1 XRD pattern of Ba$_{0.97}$Nd$_{0.0267}$Ti$_{(1-x)}$W$_x$O$_3$ ceramics with $x = 0.00$ and 0.05. Open circles correspond to the X-ray diffraction data and the lines are theoretical fits to the observed X-ray data. Rietveld analysis results for $x = 0.05$ sample. Vertical bars are the Bragg reflections for the *P4mm* space group. The pattern difference between the observed data and the theoretical fit is shown at the bottom.

Table 1 Refined structural parameters for $Ba_{0.97}Nd_{0.0267}Ti_{(1-x)}W_xO_3$ (x = 0.00 and 0.05) after the Rietveld refinements of the XRD pattern

$Ba_{0.97}Nd_{0.0267}Ti_{(1-x)}W_xO_3$	$x = 0.00$	$x = 0.05$
Cell parameters		
$a = b$ (Å)	3.9973(6)	3.997(1)
c (Å)	4.0117(0)	4.014(0)
V (Å^3)	64.14(2)	64.136
c/a	1.0036	1.0042
Discrepancy factors		
R_p (%)	7.5	8.34
R_{wp} (%)	9.46	10.7
χ^2	1.79	2.454
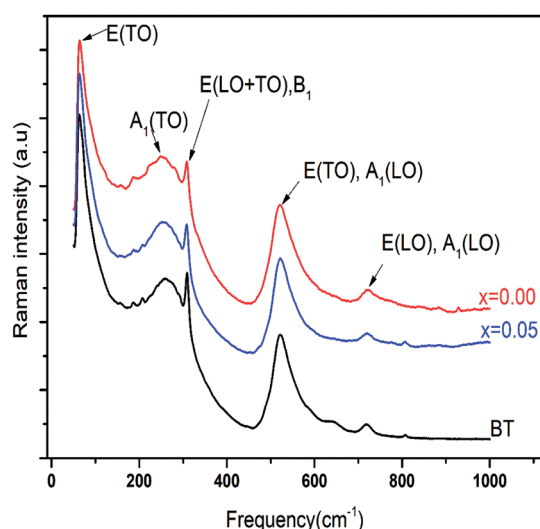
Fig. 2 Raman spectra of BT and $Ba_{0.97}Nd_{0.0267}Ti_{(1-x)}W_xO_3$ ceramics with x = 0.00 and 0.05 at room temperature.

$Ba_{0.97}Nd_{0.0267}TiO_3$ are not significantly different from that of the undoped compound meanwhile an interesting modification of local vibrational dynamics introduced by the structural distortion and slight change in local symmetry of the pure sample can be observed. However, the spectra are similar to that of Raman active modes of $BaTiO_3$ in tetragonal phase,[14] which is consistent with our XRD result. In order to determine the exact peak frequencies of the different Raman active modes, we fitted the Raman data of the $BaTiO_3$ and $Ba_{0.97}Nd_{0.0267}Ti_{(1-x)}W_xO_3$ ceramics, which is shown in Fig. 3. The proposed assignments and other observed mode wave numbers are summarized in Table 2, which compare the patterns observed in this study with those prelifted according to the literature.[15–18]

As shown in Fig. 3a, the sample BT is characterized, in the low- to mid wavenumber region, by peaks at 64.7 and 80.4 cm^{-1} attributed to the A-site vibration in the pervoskite,[17] a broad $A_1(TO_2)$ mode at 269.7 cm^{-1} assigned to TiO_6 bending vibrations, an interference dip $A_1(TO_1)$ anti-symmetric mode at 187.5 cm^{-1} and a mode at 309.3 cm^{-1}, which appears only in the presence of a long-range ferroelectric phase.[19] Modes $A_1(TO_1)$ and $A_1(TO_2)$ suggesting the existence of single-domain single-crystals of tetragonal BT.[20]

In the high-wavenumber region (>500 cm^{-1}), vibrations associated with the oxygen octahedra are present. The $A_1(TO_3)$ mode at 520.8 cm^{-1} corresponds to the O–Ti–O symmetric stretching vibration of the octahedral $[TiO_6]$ cluster (inset Fig. 3a).

Modes observed at 555.1 and 639.6 cm^{-1} are dominated by vibrations involving mainly oxygen displacements[21] and the last peak occurs only in small particle size samples.[22] The peak at 719.1 cm^{-1} can be labeled as $A_1(LO_3)$ + $E(LO_4)$ mode associated with distortion of BO_6 octahedra in ferroelectric phase. Both bands observed at 309.3 cm^{-1} and 719.1 cm^{-1} clearly confirm the presence of the tetragonal phase of ferroelectric BT.[23] Whereas the peak at 807.5 cm^{-1} corresponds to the $A_1(LO)$ + $E(LO_3)$ mode.[24]

Additionally, as shown in Fig. 3b, a band of 768.5 cm^{-1} $[A_{1g}]$ appeared at x = 0.00. Since the A_{1g} octahedral breathing mode (related to oxygen octahedral vibration) is Raman inactive in pure BT (Fig. 3a),[25] the 768.9 cm^{-1} band in this research indicates that Ti–O structure must be modified and the oxygen octahedron became asymmetric, which was consistent with the research of Pokorny et al.[26] In this research, the 768.9 cm^{-1} band is responsible for the substitution of Nd^{3+} at Ba site and accompanied the formation of oxygen vacancies,[27] which can be described as:

$$Nd \xrightarrow{Ba} Nd'_{Ba} + V_o^{\cdot\cdot}$$

A very weak band at 987 cm^{-1} is characteristic of the second-order Raman Spectra for BT.[28]

In the x = 0.05 sample, Fig. 3c, the incorporation of W^{6+} ions into the B-site induced clear changes in by the experimental Raman spectrum explained by the existence of the impurity in our compound ($BaWO_4$) confirmed the two peaks observed at 884.9 and 928.6 cm^{-1} in the high wavelengths. In addition in the low wavelengths, the impurity existence a peaks at 109.9, 156.4, 321.6 and 374.7 cm^{-1} was confirmed also by the observation of Jayaraman et al.,[29]

Moreover, as shown in Fig. 3b and c, the position of A_g mode dramatically moved from 768.5 cm^{-1} for x = 0.00 to 763.2 cm^{-1} for x = 0.05, which is connected to the cation disorder/order usually observed in $AB'_{1/3}B''_{2/3}O_3$ complex perovskites such as $Ba(Mg_{1/3}Nb_{2/3})O_3$ ceramic.[30] The substitution of W^{6+} on the B-site may enhance the driving force for the short range order (SRO). These results agree well with the results in the XRD (Fig. 1) patterns from the variation of c/a ratio and the volumes of cell parameter of x = 0.00 and x = 0.05 (Table 1).

In order to better understand the optical properties, we studies the FTIR spectra in the range 450–4000 cm^{-1} of the $Ba_{0.97}Nd_{0.0267}Ti_{(1-x)}W_xO_3$ (x = 0.00 and x = 0.05) ceramics. These spectra are presented in Fig. 4. All samples exhibit a main transmission band around 515 cm^{-1} attributed to stretching vibrations of Ti–O octahedra. According to the literature, this prominent absorption band corresponds to the bending and stretching vibrations of the TiO_6 octahedron at site B of the ABO_3 perovskite.[31] The appearance of the band at 809 cm^{-1} for the x = 0.05 sample is associated with the stretching vibrations
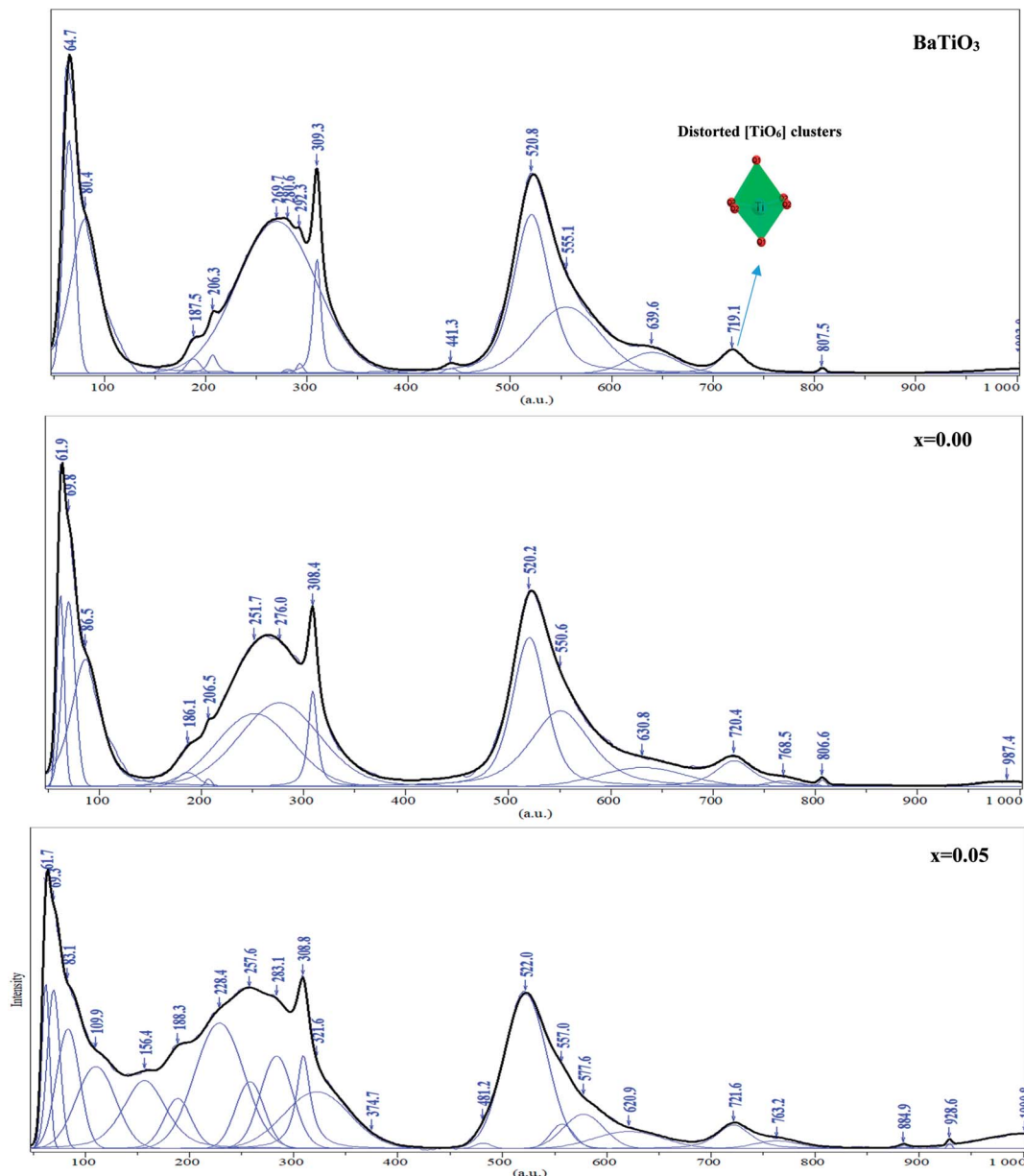
Fig. 3 Raman spectra deconvolution of the region between 50 and 1000 cm^{-1} at room temperature for BaTiO$_3$, Ba$_{0.97}$Nd$_{0.0267}$Ti$_{(1-x)}$W$_x$O$_3$ ($x = 0.00$ and $x = 0.05$).

of W–O of impurity BaWO$_4$.[32] These results confound the results found in the Raman spectrum (Fig. 3).

The only difference between the two compounds is summarized by the shift of the respective modes to the low frequencies with the incorporation of tungsten at B site, which can be explained by taking into consideration the random grain orientations in the ceramics and the grain size of the powder,[33] as given in an earlier publication[34] (such as the grain size D_{SEM} = 175.35 nm for $x = 0.00$ and D_{SEM} = 152.12 nm for $x = 0.05$). This interpretation has been included in many cases of perovskite systems as reported by Suchanicz et al.[35] that the Raman and also FTIR lines in ceramics, resulting from mode mixing and long range electrostatic force effects, shift remarkably to higher/lower values depending upon the size of the grains and depolarization fields. These observations report the correlation

behavior between the structural and optical properties of the compounds which can be admitted to explain our results and their causes. In fact, additional insertion of tungsten cation in the compounds induced a modification in grain size, and a shift of the Raman and FTIR measurements.

The absorption spectra of Ba$_{0.97}$Nd$_{0.0267}$Ti$_{(1-x)}$W$_x$O$_3$ ($x = 0.00$ and $x = 0.05$) ceramics in the visible and near infrared region at room temperature are shown in Fig. 5. The assignment of the observed absorption bands has been made according to the earlier studies on Nd^{3+} ions doped pervoskite ceramics.[36] Both spectra consist of seven absorption bands located at 885, 804, 745, 681, 586, 522 and 474 nm, which correspond to the 4f–4f transition of Nd^{3+} ions from the ground state $^4I_{9/2}$ to the excited states $^4F_{3/2}$, ($^4F_{5/2}$ + $^2H_{9/2}$), ($^4F_{7/2}$ + $^4S_{3/2}$), $^4F_{9/2}$, ($^4G_{5/2}$ + $^2G_{7/2}$), ($^4G_{9/2}$ + $^2K_{13/2}$ + $^4G_{7/2}$) and

Table 2 Mode frequencies of the Raman bands in the $BaTiO_3$ and $Ba_{0.97}Nd_{0.0267}Ti_{(1-x)}W_xO_3$ for ($x = 0.00$ and 0.05) ceramics obtained from the deconvolution of the Raman spectra at room temperature

Raman modes (cm^{-1})	BT	$Ba_{0.97}Nd_{0.0267}Ti_{(1-x)}W_xO_3$		BT single crystal Freire et al.[18]	Pure BT Shiratori et al.[19]
		$x = 0.00$	$x = 0.05$		
A site vibration (Ba–O/Nd–O)	—	61.7	61.9	—	59
E(TO1)	64.7	69.3	69.8	—	66
A$_1$(LO1)	80.4	83.1	86.5	38	38
E(TO2)	187.5	186.1	188.3	180	180
	206.3	206.5	228.4	189	—
A$_1$(TO2)	269.7	251.7	257.6	276	250
	280.6	276.0	283.1	—	270
E(TO2 + LO2)	309.3	308.4	308.8	308	306
B$_1$	—	—	321.6	308	—
A$_1$(LO2) + E(LO3)	441.3	—	481.2	466	470
A$_1$(TO3)	520.8	520.2	522.0	512	520
	555.1	550.6	557.0	—	—
	639.6	630.8	620.9	—	—
E(LO4)	719.1	720.4	721.6	722	720
A$_1$(LO3)	—	768.5	763.2	740	838
A$_1$(LO) + E(LO3)	807.5	806.6	—	—	800
ν_{BaWO4}	—	—	884.9	—	—
ν_{BaWO4}	—	—	928.6	—	—
Second order	—	987.4	—	—	—

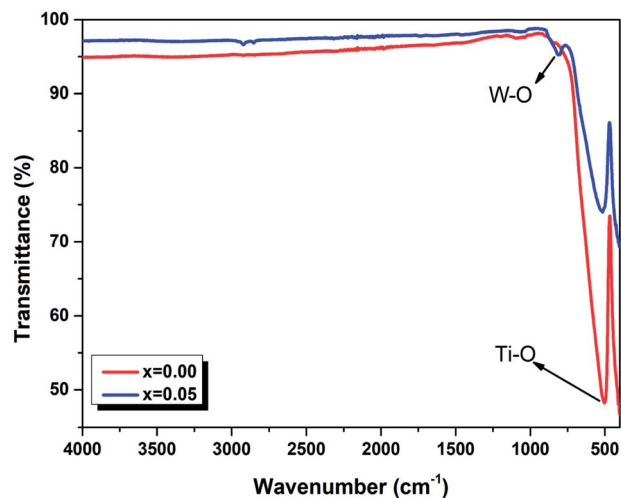**Fig. 4** FTIR spectra of $Ba_{0.97}Nd_{0.0267}Ti_{(1-x)}W_xO_3$ ($x = 0.00$ and $x = 0.05$) ceramics at room temperature.

Fig. 6 Energy band gap as a function of $Ba_{0.97}Nd_{0.0267}Ti_{(1-x)}W_xO_3$ ($x = 0.00$ and 0.05) ceramics.

($^2D_{3/2} + {}^2G_{11/2} + {}^2G_{9/2} + {}^2K_{15/2}$) respectively.[37] The position and intensity ($^4G_{5/2} + {}^2G_{7/2}$) of rare earth ions is higher for than other transitions which are found to be very sensitive to the environment of the rare earth ion. This transition is known as hypersensitive transition (at 580 nm) because of its strong dependency on the environment of the neodymium ions.[38]

The absorption spectra were found similar for the different concentrations of WO_3 with a change in the intensities of the absorption bands. However, a small shift towards longer wavelengths of the position of absorption bands was observed. This shift is related to the variation of the mean radius of the 4f layer of the rare earth ion.[39]

To determine the optical band gap energies of the samples, we made use of the following relation, proposed by Tauc,[40] Davis and Mott:[41]
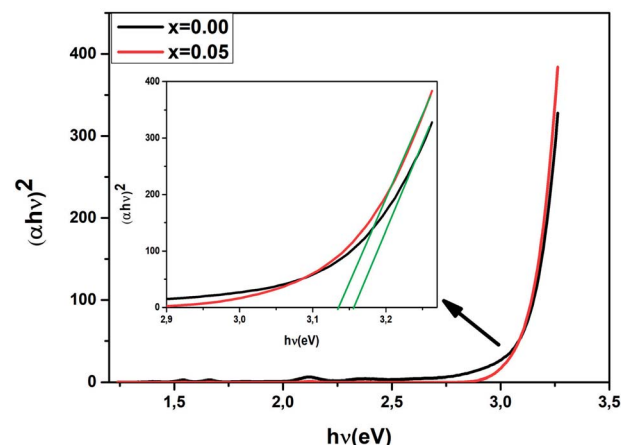
Table 3 Band gap energy (E_g), Urbach energy (E_u) and number of photons for $Ba_{0.97}Nd_{0.0267}Ti_{(1-x)}W_xO_3$ ($x = 0.00$ and 0.05) ceramics

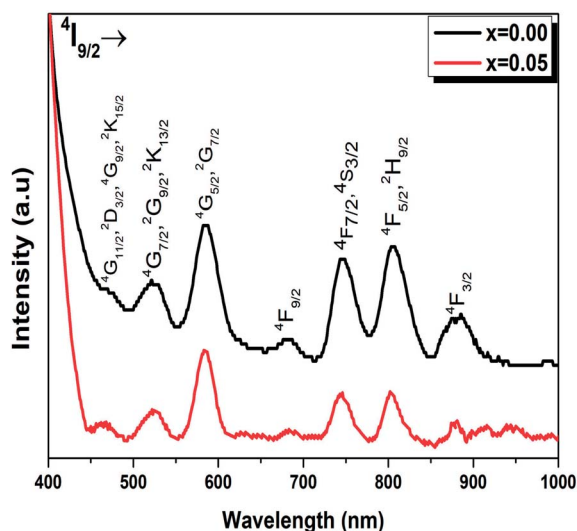|	$x = 0.00$	$x = 0.05$
E_g(eV)	3.15	3.13
E_u(eV)	0.16	0.19
Transitions Nd^{3+} in BNT_x	Number of photons	
$^4F_{3/2} \rightarrow {}^4I_{9/2}$	1.53	1.5
$^4F_{3/2} \rightarrow {}^4I_{11/2}$	1.47	1.4
$^4F_{3/2} \rightarrow {}^4I_{13/2}$	1.49	1.7

$$\alpha(\nu) = \frac{B(h\nu - E_g)^n}{h\nu} \qquad (1)$$

Fig. 5 Absorption spectrum of $Ba_{0.97}Nd_{0.0267}Ti_{(1-x)}W_xO_3$ ($x = 0.00$ and $x = 0.05$) ceramics in the visible-NIR region at room temperature. All transitions start from the $^4I_{9/2}$ ground state to the indicated levels.
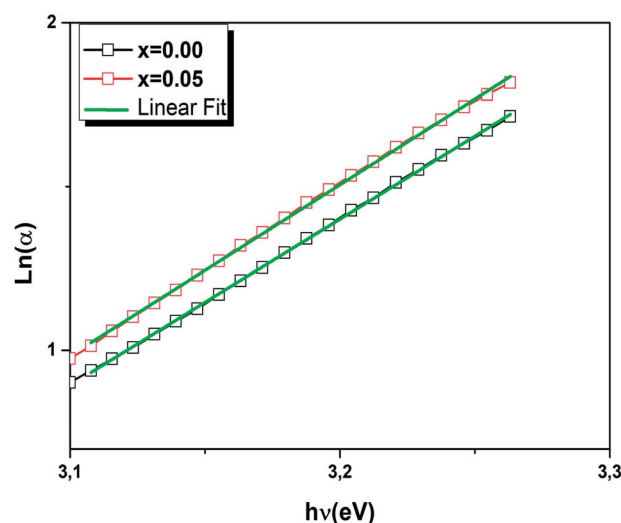

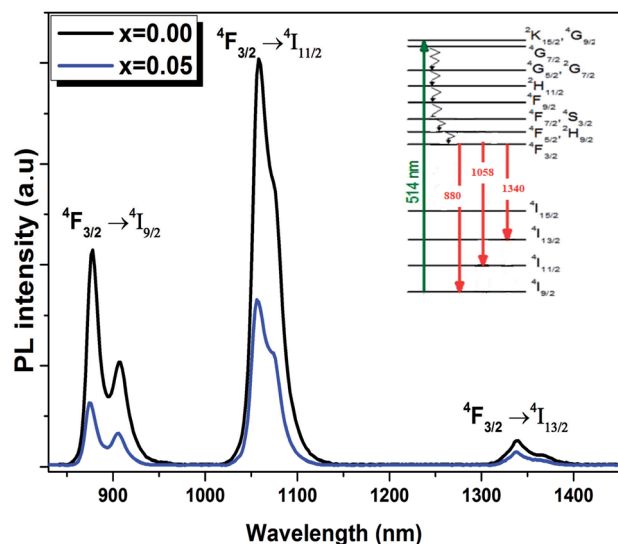**Fig. 7** Plot $\ln(\alpha)$ *versus* photon energy ($h\nu$) for $Ba_{0.97}Nd_{0.0267}Ti_{(1-x)}W_xO_3$ ($x = 0.00$ and 0.05).

Fig. 8 Down-conversion emission spectra of the $Ba_{0.97}Nd_{0.0267}$-$Ti_{(1-x)}W_xO_3$ ceramics excited at 514 nm at room temperature. Inset schematic energy level scheme of Nd^{3+} ions in $Ba_{0.97}Nd_{0.0267}Ti_{(1-x)}$-$W_xO_3$ (x = 0.00 and x = 0.05).

here B is a constant, and E_g is the optical gap energy, n is an exponent which depends on the nature of the electronic transitions responsible for the absorption. Indeed, two kinds of optical transitions near the fundamental absorption edge may occur. These are usually named direct and indirect transitions. The parameter n is equal to 1/2 for allowed direct transitions, 3/2 for direct forbidden transitions, 2 for allowed indirect transitions and 3 for forbidden indirect transitions. However, it is likely to consider only direct transitions for most of the pervoskite ceramics.[42,43] Therefore, eqn (1) becomes:

$$(\alpha h\nu)^2 = B(h\nu - E_g) \qquad (2)$$

We have plotted the variation of $(\alpha h\nu)^2$ against $(h\nu)$ for all the samples. The values of direct optical band gap (E_g) for $Ba_{0.97}$-$Nd_{0.0267}Ti_{(1-x)}W_xO_3$ (x = 0.00 and x = 0.05) samples were obtained, as shown in Fig. 6, by extrapolating the straight line on the curves to $h\nu$ axis at $(\alpha h\nu)^2 = 0$. The E_g values are presented in Table 3. These results are close to those reported by Jiang et al.[44] for the sample $BaTiO_3$: 2% Nd^{3+} films (3.49 eV), M. Dhanalakshmi et al.[45] for $BaTiO_3$: 1%Nd^{3+} nanophosphors (3.29 eV), Kappadan et al.[46] $BaTiO_3$ (3.12 eV) prepared by polymeric complex method.[47]

The width of defect bands formed in the band gap is associated with Urbach energy E_u.[48] It could be determined from the following eqn:
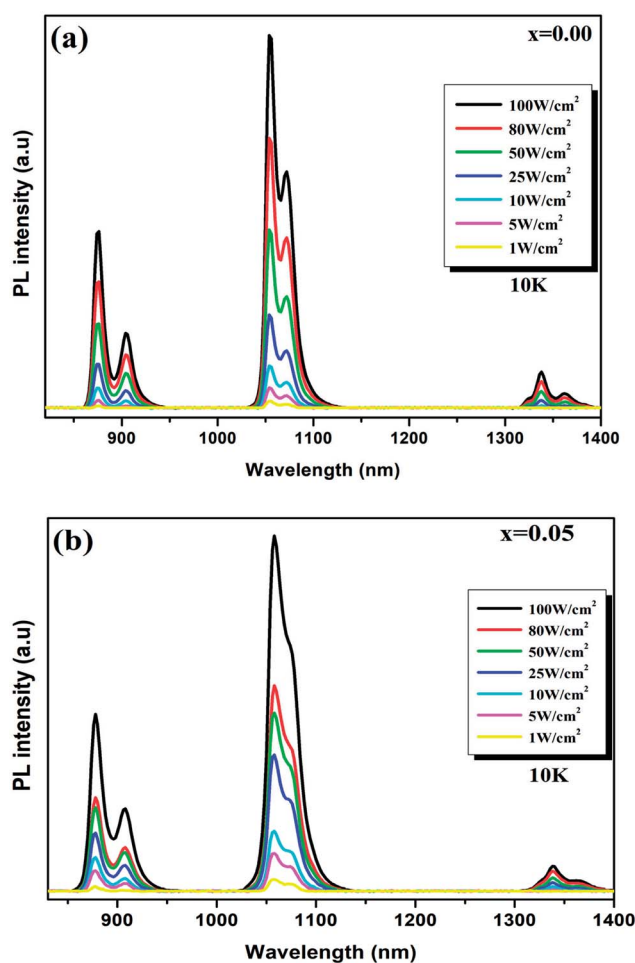

Fig. 9 (a) and (b) PL intensity of $Ba_{0.97}Nd_{0.0267}Ti_{(1-x)}W_xO_3$ (x = 0.00 and x = 0.05) at 10 K at different excitation power densities, respectively.
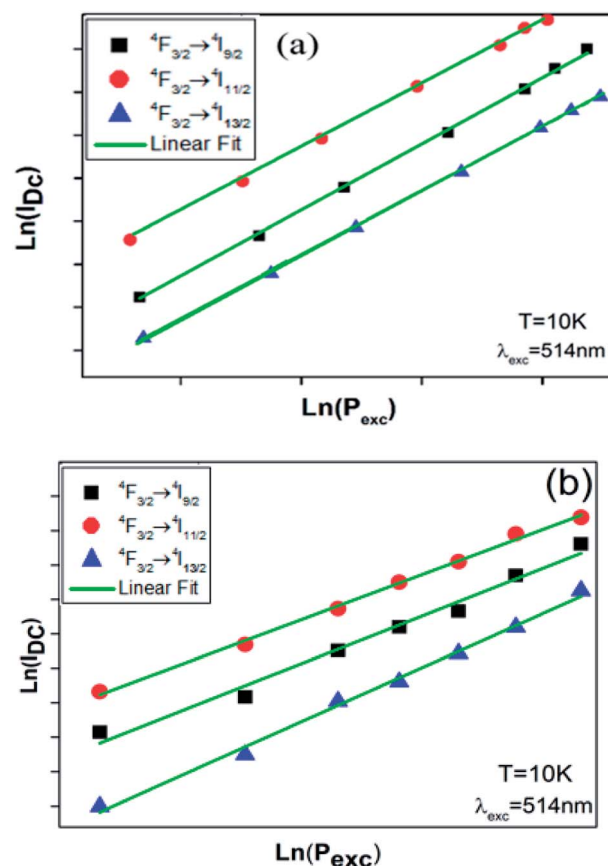

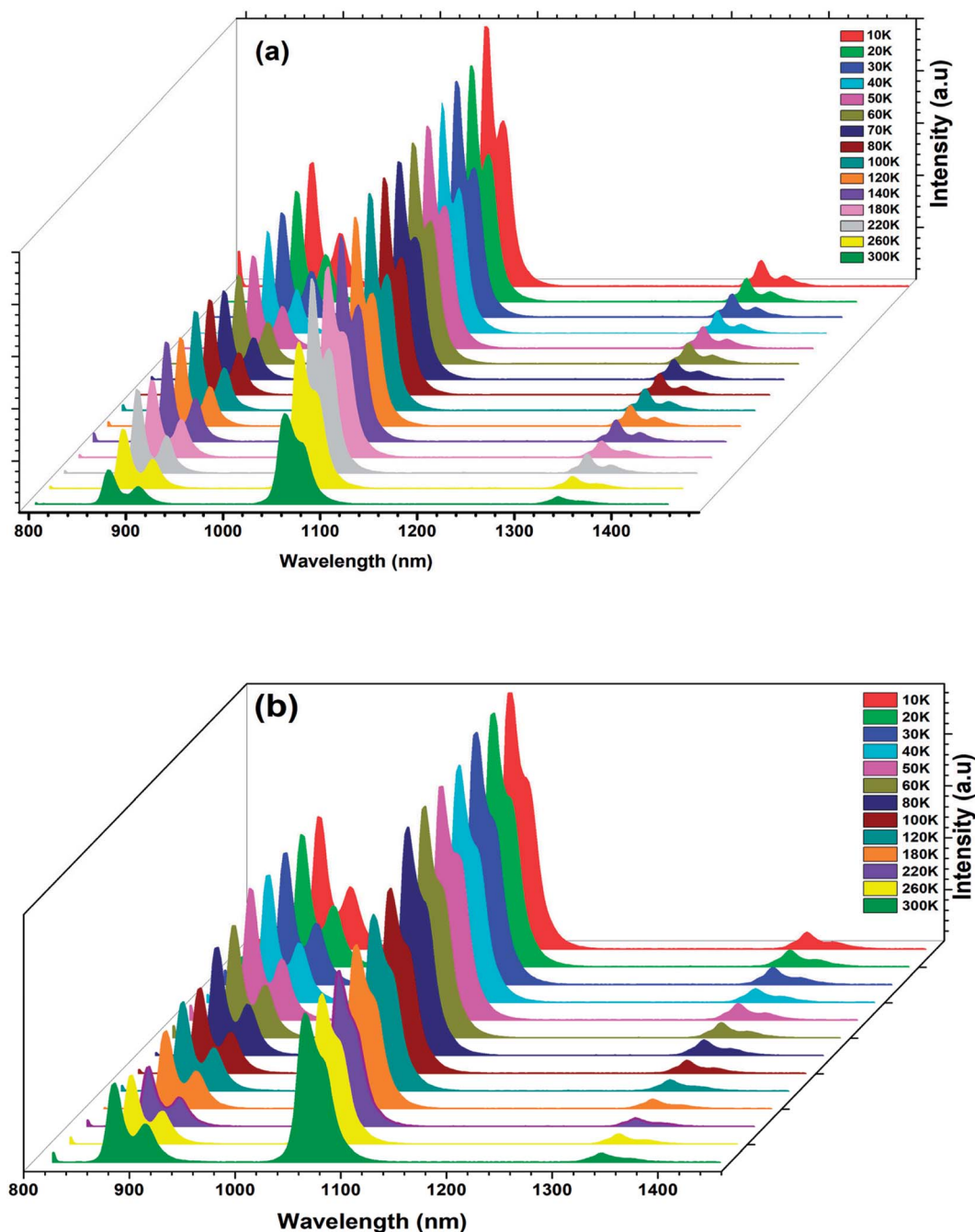Fig. 10 (a) and (b) log–log plot of PL intensity versus excitation power density for x = 0.00 and x = 0.05 at 10 K.

Fig. 11 (a) and (b) Temperature-dependent PL emission spectra of the $Ba_{0.97}Nd_{0.0267}Ti_{(1-x)}W_xO_3$ ($x = 0.00$ and $x = 0.05$) ceramics.

$$\alpha = \alpha_0 \exp\left(\frac{h\nu}{E_u}\right) \quad (3)$$

The Urbach energy E_u was calculated by plotting $\ln(\alpha)$ *versus* photon energy ($h\nu$) (Fig. 7).

The E_u values are also summarized in Table 3. A slight increase in the Urbach energy values is noticed with the addition of W^{6+} ions.

Finally, when W^{6+} is incorporated in $Ba_{0.97}Nd_{0.0267}Ti_{(1-x)}W_xO_3$ ceramic, the band gap decreases and the Urbach energy increases. This result clearly demonstrates the formation of intermediate states in the band gap and a reduction in the gap values.

The room temperature emission spectra of the $Ba_{0.97}Nd_{0.0267}Ti_{(1-x)}W_xO_3$ ($x = 0.00$ and $x = 0.05$) ceramics, are shown in Fig. 8. The emission spectra consists of three centered large and non-symmetric bands, which mainly originates from the radiative transition due to the electrical dipole transitions among 4f–4f of Nd^{3+} ions, near 880, 1058 and 1340 nm. These emission bands correspond to $^4F_{3/2} \rightarrow {}^4I_{9/2}$, $^4F_{3/2} \rightarrow {}^4I_{11/2}$ and $^4F_{3/2} \rightarrow {}^4I_{13/2}$, respectively.

As seen from Fig. 8, the PL intensities of $Ba_{0.97}Nd_{0.0267}$-$Ti_{(1-x)}W_xO_3$ decreased with the addition of W^{6+} ions. The existence of W^{6+} makes it possible to find impurity $BaWO_4$, which results in a contraction of the lattice. In this condition, the Nd^{3+} ions will get much closer to each other, which enhance their interaction and results in the exhaustion of their emission by non-radiative energy transfer. The experimental results strongly showed that photoluminescence is directly related to the structural disorder. Similar results were reported by Q. Zhang *et al.*, in $(K_{0.5}Na_{0.5})NbO_3 : Sm^{3+}/Zr^{4+}$ materials.[49] For the present sample, W^{6+} ion-doped $Ba_{0.97}Nd_{0.0267}TiO_3$ at B sites induce the local lattice distortion, confirmed by the results obtained in Raman Fig. 3. Nevertheless, the experimental data (the decrease PL intensities and no shift of emission peaks) show that W^{6+} substitution does give rise to distinct influence on the emission intensity and crystal structure.

The energy level diagram of Nd^{3+} ions is given in the inset of Fig. 8. Under the excitation of 514 nm, the Nd^{3+} ions are excited from ground state $^4I_{9/2}$ to $^4G_{9/2}$-$^2K_{15/2}$ levels. The population in the $^4G_{9/2}$, $^2K_{15/2}$ levels decays non-radiatively by fast and successive multiphonon relaxation processes to the $^4F_{3/2}$ state, from which infrared emission arises at 880, 1058 and 1340 nm corresponding to $^4F_{3/2} \rightarrow {}^4I_{9/2}$, $^4F_{3/2} \rightarrow {}^4I_{11/2}$ and $^4F_{3/2} \rightarrow {}^4I_{13/2}$ transitions, as shown in Fig. 8.

To produce the DC in the BNT_x ceramics it is important to understand the DC emissions during the excitation power.

The DC PL spectra of the BNT_x ceramics under the excitation of 514 nm laser for the different excitation power, are presented in Fig. 9. It is noteworthy that the PL intensity increases with the increment of excitation power.

In order to identify the process behind the observed emissions, we have measured the emissions intensities as a function of excitation power at 10 K. The relationship between DC emission intensity (I_{DC}) and the excitation power (P_{exc}) can be represented by the following formula:[50]

$$I_{DC} \propto (P_{exc})^n \qquad (4)$$

where I_{DC} is the integrated PL intensity, P_{exc} is the excitation power, and n is the number of excitation photons required in the DC process.

Fig. 10 shows the logarithm variation of the integrated emissions intensities of the down-converted fluorescence *versus* the excitation power at 10 K for BNT_x ceramics. A linear fitting of the experimental data gave slopes representing the number of excitation photons required for the corresponding down-converted emissions. The fitting n values are listed in Table 3. This results indicate that two photons are required to create these mechanisms.

Generally, the emission intensity decreases gradually with increasing temperature, due to the enhancement of the non-radiative transition probability while the phosphor is heated.[51]

The temperature-dependent PL emission spectra of the BNT_x ($x = 0.00$ and $x = 0.05$) under 514 nm of excitation wavelength is depicted in Fig. 11.

From the emission spectra, we notice that the PL intensity gradually decreased with increasing the temperature from 10 to 300 K and the overall shape and position of the emission spectra remained unchanged as the temperature is increased.

This decrease is due to the temperature-dependence of the electron–phonon interaction. Mot is to say part the phonon vibrations increase with the increase of temperature.

To further understand the thermal activation energy can be determined from an Arrhenius plot of the integrated intensity of the emission against reciprocal temperature as given by:[52]

$$I(T) = \frac{I_0}{1 + c \exp\left(-\dfrac{E_a}{kT}\right)} \qquad (5)$$

where I_0 and $I(T)$ are the emission intensity at the initial temperature (10 K) and the measured temperature T, c is a constant, E_a is the activation energy of thermal quenching, and k is the Boltzmann constant (8.629×10^{-5} eV K^{-1}). The plot of the normalized PL intensity *versus* $1000/k_BT$ is shown in Fig. 12.

The value of E_a obtained here using the fitting for the experimental data are found to be $E_a = 130$ meV for the $x = 0.00$ sample, and $E_a = 142$ meV for the $x = 0.05$ sample. Based on literature, the phonon energy of PLZT is about 100 meV.[53]

The E_a values are lower, which can be explained by the non-radiative transition and the good thermal stability of both
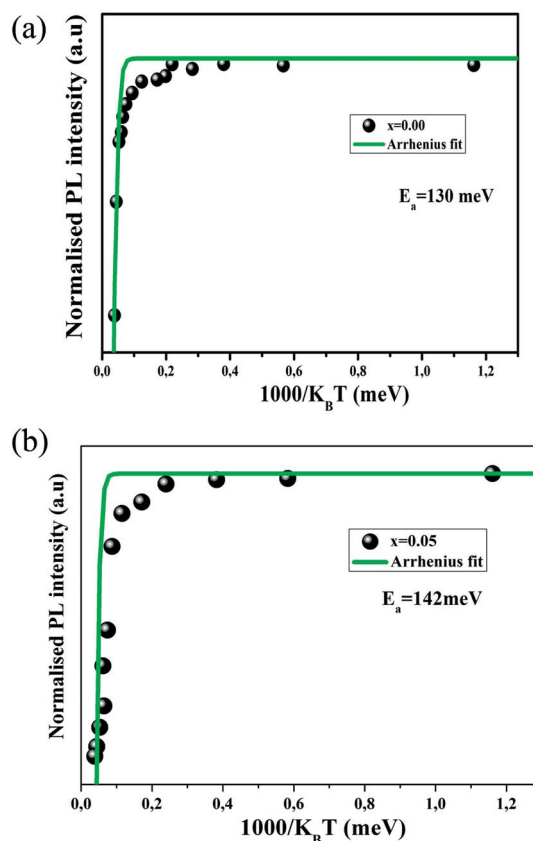

Fig. 12 (a) and (b) Evolution of the integrated intensity *versus* the inverse of the temperature (black scatters) and the corresponding best fit (continuous green line), for $x = 0.00$ and $x = 0.05$ samples, respectively.

samples.[54] It is worth pointing out that the thermal activation energies for both samples are close to the phonon energy.

Increasing the W^{6+} concentration in the host lattice led to a significant change of the optical properties and is explained by structural distortion and other parameters such as grain size. However, our investigation of this correlation between structural and optical proprieties proves that thanks to their optical sensitivity, and good thermal stability, our compounds could be good candidates for many practical applications in luminescent devices.

4. Conclusion

In this work, we have studied the structural and optical properties of $Ba_{0.97}Nd_{0.0267}Ti_{(1-x)}W_xO_3(x = 0.00$ and $x = 0.05)$ ceramic prepared by molten salt method. Raman spectroscopy revealed that all the prepared samples have perovskite phase and crystallize in the $P4mm$-tetragonal symmetry. Temperature-dependent photoluminescent spectra showed that the BNT_x ceramics exhibit good thermal stability of photoluminescence in the temperature range from 10 K to 300 K, suggesting good thermal stability of the pervoskite.

Conflicts of interest

There are no conflicts to declare.

References

1 J. H. Li, X. Z. Fu, J. L. Luo, K. T. Chuang and A. R. Sanger, Application of $BaTiO_3$ as anode materials for H_2S-containing CH_4 fueled solid oxide fuel cells, *J. Power Sources*, 2012, **213**, 69–77.

2 H. M. Huang, H. Y. Li, X. X. Wang and X. Guo, Detecting low concentration of H_2S gas by $BaTiO_3$ nanoparticle-based sensors, *Sens. Actuators, B*, 2017, **238**, 16–23.

3 Y. Okamoto and Y. Suzuki, Mesoporous $BaTiO_3/TiO_2$ Double Layer for Electron Transport in Perovskite Solar Cells, *J. Phys. Chem. C*, 2016, **120**, 13995–14000.

4 J. P. B. Silva, F. L. Faita, K. Kamakshi, K. C. Sekhar, J. A. Moreira, A. Almeida, M. Pereira, A. A. Pasa and M. J. M. Gomes, Enhanced resistive switching characteristics in $Pt/BaTiO_3/ITO$ structures through insertion of $HfO_2:Al_2O_3$ (HAO) dielectric thin layer, *Sci. Rep.*, 2017, **7**, 46350.

5 G. Singh, V. S. Tiwari, T. K. Sharma and P. K. Gupta, Temperature dependence photo-luminescence of Nd^{3+} doped PLZT ceramic, *J. Electroceram.*, 2010, **25**, 89–92.

6 C. R. Kesavulu, H. J. Kim, S. W. Lee, J. Kaewkhao, N. Wantana, E. Kaewnuam, S. Kothan and S. Kaewjaeng, Spectroscopic investigations of Nd^{3+} doped gadolinium calcium silica borate glasses for the NIR emission at 1059 nm, *J. Alloys Compd.*, 2017, **695**, 590–598.

7 K. Lemanski, A. Gagor, M. Kurnatowska, R. Pazik and P. J. Deren, Spectroscopic properties of Nd^{3+} ions in nano-perovskite $CaTiO_3$, *J. Solid State Chem.*, 2011, **184**, 2713–2718.

8 C. He, Y. Zhang, L. Sun, J. Wang, T. Wu, F. Xu, C. Du, K. Zhu and Y. Liu, Electrical and optical properties of Nd^{3+}-doped $Na_{0.5}Bi_{0.5}TiO_3$ ferroelectric single crystal, *J. Phys. D: Appl. Phys.*, 2013, **46**, 245104.

9 D. Shihua, S. Tianxiu, Y. Xiaojing and L. Guanghua, Effect of Grain Size of $BaTiO_3$ Ceramics on Dielectric Properties, *Ferroelectrics*, 2010, **402**, 55–59.

10 M. Venkateswarlu, S. k. Mahamuda, K. Swapna, M. V. V. K. S. Prasad, A. S. Rao, A. Mohan Babu, S. Shakya and G. V. Prakash, Spectroscopic studies of Nd^{3+} doped lead tungsten tellurite glasses for the NIR emission at 1062 nm, *Opt. Mater.*, 2015, **39**, 8–15.

11 M. Guzik, M. Bieza, E. Tomaszewicz, Y. Guyot, E. Zych and G. Boulon, Nd^{3+} dopant influence on the structural and spectroscopic properties of microcrystalline $La_2Mo_2O_9$ molybdate, *Opt. Mater.*, 2015, **41**, 21–31.

12 R. Bokolia, M. Mondal, V. K. Rai and K. Sreenivas, Enhanced infrared-to-visible up-conversion emission and temperature sensitivity in (Er^{3+}, Yb^{3+}, and W^{6+}) tri-doped $Bi_4Ti_3O_{12}$ ferroelectric oxide, *J. Appl. Phys*, 2017, **121**, 084101.

13 Y. R. D. Shannon, *Acta Crystallogr.*, 1976, **A32**, 751.

14 P. Xue, Y. Hu, W. Xia, H. Wu and X. Zhu, Molten-salt synthesis of $BaTiO_3$ powders and their atomic-scale structural characterization, *J. Alloys Compd.*, 2017, **695**, 2870–2877.

15 C. Chalfouh, A. Lahmar, S. Zghal, R. Hannachi, N. Abdelmoula and H. Khemakhem, Effects of lanthanide amphoteric incorporation on structural, electrical and photoluminescence properties of $BaTi_{0.925}(Yb_{0.5}Nb_{0.5})_{0.075}O_3$ ceramic, *J. Alloys Compd.*, 2017, **711**(15), 205–214.

16 H. Kaddoussi, N. Abdelmoula, Y. Gagou, D. Mezzane, H. Khemakhem and M. Elmarssi, X-ray diffraction, dielectric and Raman spectroscopy studies of $Ba_{1x}Nd_{2x/3}(Ti_{0.9}Zr_{0.1})O_3$ ceramics, *Ceram. Int.*, 2014, **40**, 10255–10261.

17 M. Zannen, A. Lahmar, M. Dietze, H. Khemakhem, A. Kabadou and M. Es-Souni, Structural, optical and electrical properties of Nd-doped $Na_{0.5}Bi_{0.5}TiO_3$, *Mater. Chem. Phys.*, 2012, **134**, 829–833.

18 J. D. Freire and R. S. Katiyar, Lattice dynamics of crystals with tetragonal $BaTi0_3$ structure, *Phys. Rev. B: Condens. Matter Mater. Phys.*, 1988, **37**, 2074.

19 Y. Shiratori, C. Pithan, J. Dornseiffer and R. Waser, Raman scattering studies on nanocrystalline $BaTiO_3$ Part I – isolated particles and aggregates, *J. Raman Spectrosc.*, 2007, **38**, 1288–1299.

20 Da-Y. Lu, X.-Y. Sun and M. Toda, A novel high-k 'Y5V' barium titanate ceramics co-doped with lanthanum and cerium, *J. Phys. Chem. Solids*, 2007, **68**, 650–664.

21 T. Mondal, S. Das, T. Badapanda, T. P. Sinha and P. M. Sarun, Effect of Ca^{2+} substitution on impedance and electrical conduction mechanism of $Ba_{1-x}Ca_xZr_{0.1}Ti_{0.9}O_3$ ($0.00 \leq x \leq 0.20$) ceramics, *Phys. B*, 2017, **508**, 124–135.

22 L. Ben Abdessalem, S. Aydi, A. Aydi, Z. Sassi, A. Maalej and H. Khemakhem, X-ray diffraction, dielectric, and Raman spectroscopy studies of $BaSrTiO_3–NaNbO_3$ ceramic, *Appl. Phys. A*, 2017, **123**, 305.

23 Z. Abdelkafi, G. Khasskhoussi, N. Abdelmoula and H. Khemakhem, Ferroelectric piezoelectric and Raman spectroscopy studies of $BaTi_{0.925}(Nb_{0.5}Yb_{0.5})_{0.075}O_3$ ceramic, *Ceram. Int.*, 2015, 14839–14844.

24 T. Mondal, S. Das, T. Badapanda, T. P. Sinha and P. M. Sarun, Effect of Ca^{2+} substitution on impedance and electrical conduction mechanism of $Ba_{1-x}Ca_xZr_{0.1}Ti_{0.9}O_3$ ($0.00 \leq x \leq 0.20$) ceramics, *Phys. B*, 2017, **508**, 124–135.

25 L. Ben Abdessalem, M. Ben Abdessalem, A. Aydi and Z. Sassi, Structural and dielectric properties of $(Ba_{1-x}Sr_x)_{0.93}Na_{0.07}Ti_{0.93}Nb_{0.07}O_3$ ceramics, *J. Mater. Sci.: Mater. Electron.*, 2017, **28**, 14264–14270.

26 J. Pokorny, U. M. Pasha and L. Ben, Use of Raman spectroscopy to determine the siteoccupancy of dopants in $BaTiO_3$, *J. Appl. Phys.*, 2011, **109**, 6–7.

27 S. Hongbing, T. M. Semkow and A. S. Bhalla, Raman spectroscopy of Mg–Ta order–disorder in$BaMg_{1/3}Ta_{2/3}O_3$, *J. Phys. Chem. Solids*, 1998, **59**, 181–195.

28 D. F. K. Hennings and H. Schreinemacher, Ca-acceptors in dielectric ceramics sintered inreductive atmospheres, *J. Eur. Ceram. Soc.*, 1995, **15**, 795–800.

29 A. Jayaraman, B. Batlogg and L. G. VanUitert, *Phys. Rev. B: Condens. Matter Mater. Phys.*, 1983, **28**, 4774.

30 Y. J. Jiang, L. Z. Zeng, R. P. Wang, Y. Zhu and Y. L. Liu, Fundamental and second-order Raman spectra of $BaTiO_3$, *J. Raman Spectrosc.*, 1996, **27**, 31–34.

31 D. Wang, R. Yu, S. Feng, W. Zheng, T. Takei, N. Kumada and N. Kinomura, Hydrothermal synthesis of perovskite-type solid solution of $(1-x)BaTiO_3 \cdot xLa_{2/3}TiO_3$, *Solid State Ionics*, 2002, **151**, 329–333.

32 T. Thongtem, A. Phuruangrat and S. Thongtem, Characterization of $MeWO_4$ (Me = Ba, Sr and Ca) nanocrystallines prepared by sonochemicalmethod, *Appl. Surf. Sci.*, 2008, **254**, 7581–7585.

33 J. Pal Singh, S. Gautam, P. Kumar, A. Tripathi, J.-M. Chen, K. H. Chae and K. Asokan, Correlation between the dielectric properties and local electronic structure of copper doped calcium titanate, *J. Alloys Compd.*, 2013, **572**, 84–89.

34 Z. Raddaoui, R. Lahouli, S. E. L. Kossi, J. Dhahri, K. Khirouni and K. Taibi, Structural and thermoelectric properties of $Ba_{0.97}Nd_{0.0267}Ti_{0.95}W_{0.05}O_3$ ceramic, *J. Alloys Compd.*, 2018, **765**, 428–436.

35 J. Suchanicz, I. J. Sumara and T. V. Kruzina, Raman and infrared spectroscopy of $Na_{0.5}Bi_{0.5}TiO_3$ – $BaTiO_3$ ceramics, *J. Electroceram.*, 2011, **27**, 45–50.

36 G. Singh, R. Selvamani, V. S. Tiwari and A. K. Karnal, Spectroscopic investigations of Nd^{3+} doped PLZT ceramics on the basis of Judd–Ofelt theory, *J. Lumin.*, 2017, **192**, 1084–1088.

37 M. Zannen, A. Lahmar, M. Dietze, H. Khemakhem, A. Kabadou and M. Es-Souni, *Mater. Chem. Phys.*, 2012, **134**, 829–833.

38 T. Wei, Y. Tian, C. Tian, X. Jing, M. Cai, J. Zhang, L. Zhang and S. Xu, *J. Alloys Compd.*, 2015, **618**, 95–101.

39 G. H. Beall and D. A. Duke, in *Glass Sci. Technol*, ed. D. R. Uhlmann and N. J. Kreidl, New York, Academic Press, 1983, vol. 1, p. 403.

40 J. Tauc, *J Optical Properties of Solids*, ed. F. Abeles, NorthHolland, Amsterdam, 1970, vol. 22, p. 903.

41 E. A. Davis and N. F. Mott, *Philos. Mag.*, 1970, **22**, 903.

42 D. K. Singh, K. Mondal and J. Manam, *Ceram. Int.*, 2017, **43**, 13602–13611.

43 F. Belkhiria, F. I. H. Rhouma, S. Hcini, M. Daoudi, H. Gammoudi, M. Amlouk and R. Chtourou, Polycrystalline $La_{0.8}Sr_{0.2}GaO_3$ perovskite synthesized by sol-gel process along with temperature dependent photoluminescence, *J. Lumin.*, 2017, **181**, 1–7.

44 W. Jiang, W. Cai, Z. Lin and C. Fu, Effects of Nd-doping on optical and photovoltaic properties of barium titanate thin films prepared by sol–gel method, *Mater. Res. Bull.*, 2013, **48**, 3092–3097.

45 M. Dhanalakshmi, H. Nagabhushana, S. C. Sharma, R. B. Basavaraj, G. P. Darshan and D. Kavyashree, *Mater. Res. Bull.*, 2018, **102**, 235–247.

46 S. Kappadan, T. W. Gebreab, S. Thomas and N. Kalarikkal, *Mater. Sci. Semicond. Process.*, 2016, **51**, 42–47.

47 Z. Li, H. Xue, X. Wang and X. Fu, Characterizations and photocatalytic activity of nanocrystalline $La_{1.5}Ln_{0.5}Ti_2O_7$ (Ln = Pr, Gd, Er) solid solutions prepared *via* a polymeric complex method, *J. Mol. Catal.*, 2006, **260**, 56–61.

48 F. Urbach, The Long-Wavelength Edge of Photographic Sensitivity and of the Electronic Absorption of Solids, *Phys. Rev.*, 1953, **92**, 1324.

49 Q. Zhang, K. Chen, L. Wang, H. Sun, X. Wangc and X. Hao, A highly efficient, orange light-emitting $(K_{0.5}Na_{0.5})NbO_3:Sm_{3+}/Zr_{4+}$ lead-free piezoelectric material with superior water resistance behavior, *J. Mater. Chem. C*, 2015, **3**, 5275.

50 L. Luo, P. Du, W. Li, W.Tao and H. Chen, Effects of Er doping site and concentration on piezoelectric, ferroelectric,and optical properties of ferroelectric $Na_{0.5}Bi_{0.5}TiO_3$, *J. Appl. Phys.*, 2013, **114**, 124104.

51 S. Murakami, M. Morita, M. Herren, T. Sakurai and D. Rau, Near-infrared luminescence and spectral anomalyin PLZT ceramics doped with Nd_3^+, Er_3^+, $Yb_3^+$and Cr_5^+ ions at low temperatures, *J. Lumin.*, 2000, **87–89**, 694–696.

52 B. Smiri, I. Fraj, F. Saidi, R. Mghaieth and H. Maaref, Effect of piezoelectric field on type II transition in InAlAs/InP (311) alloys with different substrate polarity, *J. Alloys Compd.*, 2018, **736**, 29–34.

53 G. Singh, V. S. Tiwari, T. K. Sharma and P. K. Gupta, Temperature dependence photo-luminescence of Nd^{3+}doped PLZT ceramic, *J. Electroceram.*, 2010, **25**, 89–92.

54 J. Rihani, V. Sallet, N. Yahyaoui, J. C. Harmand, M. Oueslati and R. Chtourou, Interdot carrier's transfer *via* tunneling pathway studied from Photoluminescence spectroscopy, *J. Lumin.*, 2009, **129**, 251–255.